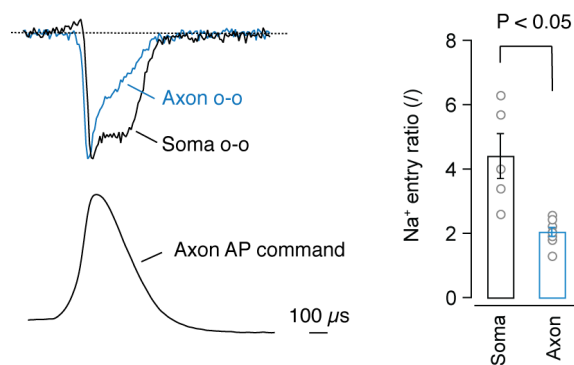*Supplementary Figures* and **Table** to the article;

State- and location-dependence of action potential metabolic cost in cortical pyramidal neurons

Stefan Hallermann, Christiaan P.J. de Kock, Greg J. Stuart and Maarten H. P. Kole
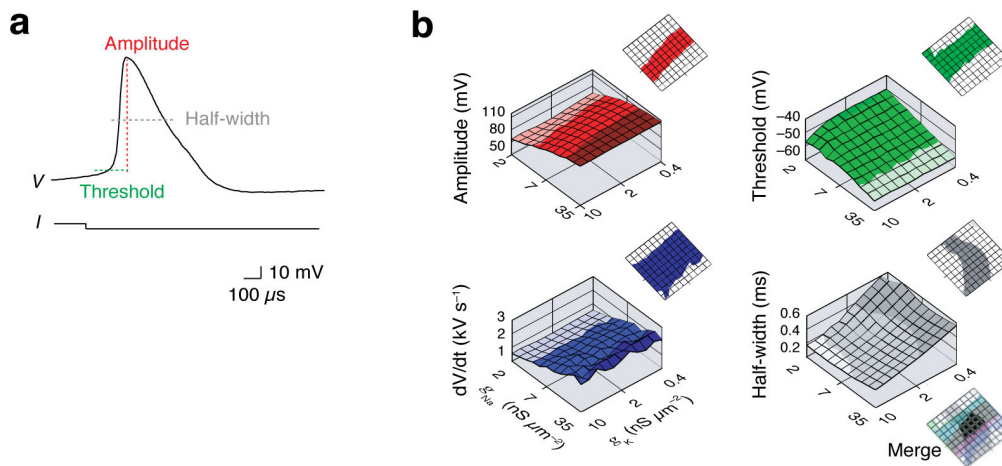
Supplementary Figures

Supplementary Figure 1. Fast kinetics of axonal Na$^+$ currents reduces the Na$^+$ excess

Left, To test whether Na$^+$ current kinetics during AP waveforms are different between subcellular compartments, identical AP command waveforms (from the axon) were applied to somatic ($n = 5$, black) or axonal outside-out patches ($n = 8$, blue). Na$^+$ currents inactivated slower in the somatic region. *Right,* Quantification of the Na$^+$ entry ratios revealed 2-fold larger ratios in somatic outside-out recordings (*t*-test $P < 0.05$). These data are consistent with the observed hyperpolarized axonal Na$^+$ channel voltage-dependence and the more rapid activation and inactivation kinetics[1-3].
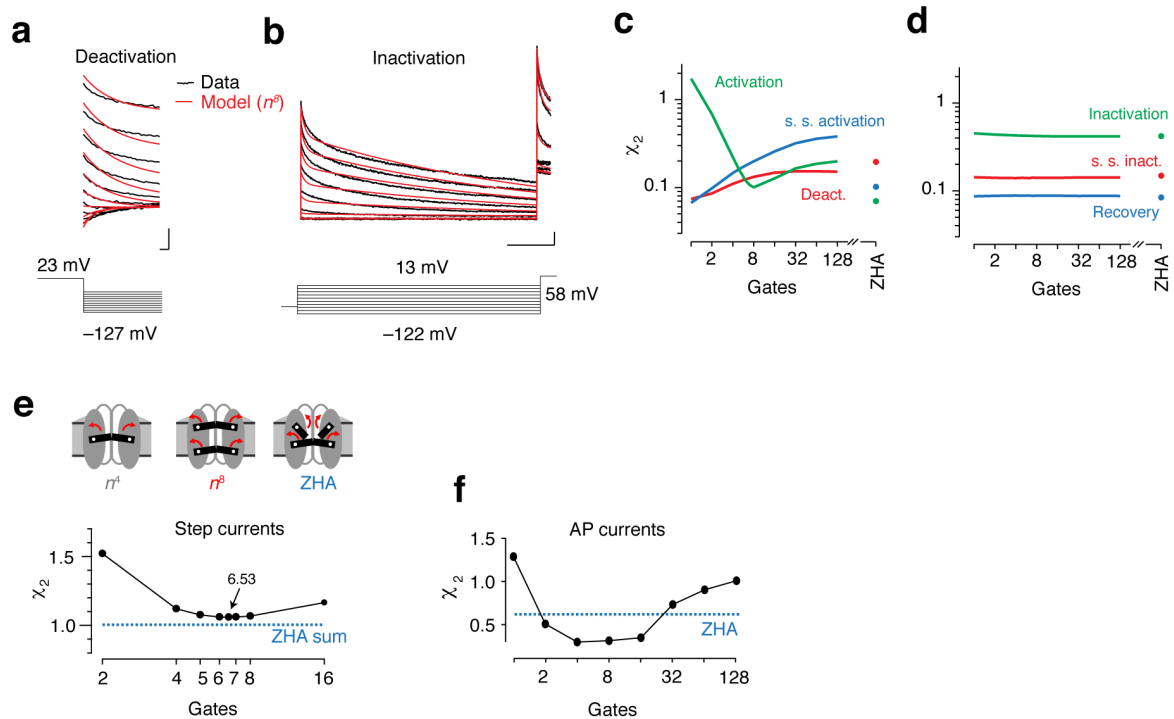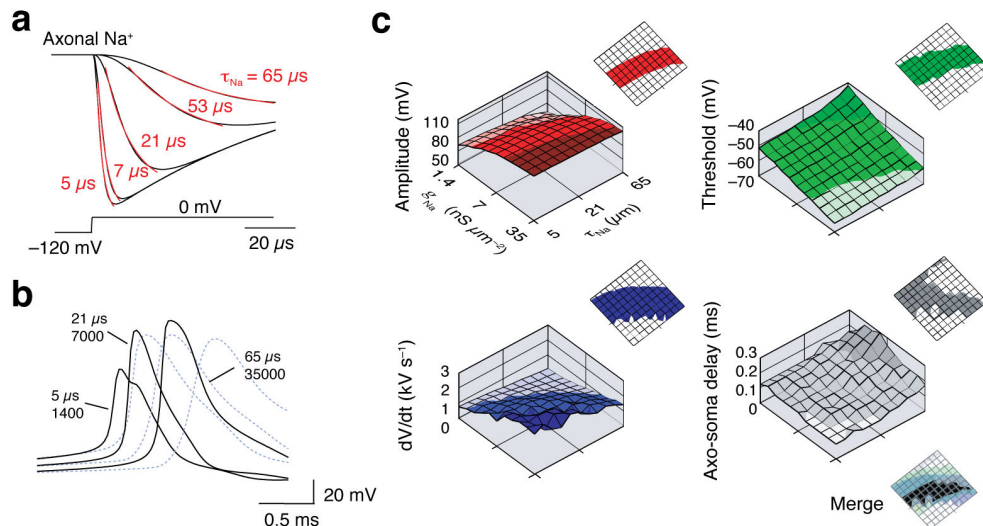
Supplementary Figure 2. Fast-activating axonal K$^+$ currents can be well described by 8-gate HH models

(**a - b**) Deactivation and inactivation currents (black) superimposed with predictions of a Hodgkin-Huxley (HH) model (red) with eight activation gates and two different inactivation kinetics. The voltage protocols are indicated below. (**c, d**) Systematic comparison of the ability of the models to predict the experimental data. The differences between the model predictions and the experimental data (χ^2, sum of squared differences; s. s., steady state) are plotted for the HH models with different numbers of activation gates, as well as for the state-model with four subunits each with two sequential activation steps (ZHA, Zagotta-Hoshi-Aldrich model[4]). (**e**) *Top,* Schematic illustration of one or two independent activation gates per subunit (n^4 and n^8, corresponding to 4 and 8 activation gates per channel) and two dependent, i.e. subsequent, activation gates per subunit of the ZHA model. *Bottom*, the global χ^2–value (black) is the sum of six χ^2–values from the data sets for HH models with 2 to 16 activation gates during step-evoked currents. If the number of activation gates is used as a free parameter, 6.53 was optimal. (**f**) χ^2–value of the simulated rising phase with the experimental rising phase during AP-evoked currents for the HH models and the ZHA model (see **Fig. 4b**).

Supplementary Figure 3. Na$^+$ and K$^+$ channel densities are high in the AIS of cortical pyramidal neurons

(**a**) Target parameters for assessment of the AIS spike shape. (**b**) Evaluation of the indicated AIS AP parameters in models with different $\overline{g}_{Na}$ and $\overline{g}_K$. In addition, the same plots are shown as viewed from top with the darker area indicating values that are within the target range (peak amplitude range: 90 – 110 mV; rate-of-rise range; 0.8 to 2 kV s^{-1}; threshold range: –58 to –52 mV and half-width range; 250 – 400 μs). *Right bottom,* the overlap of the four target ranges is shown in black (Merge).

Supplementary Figure 4. Rapid activation kinetics can not compensate for lower AIS Na$^+$ channel densities

(**a**) It has recently been suggested that axonal $\overline{g}_{Na}$ may be overestimated since the rapid activation kinetics of Na$^+$ channels are close to the maximum temporal resolution of voltage-clamp amplifiers and thus difficult to record accurately[3, 5]. We therefore explored whether $\overline{g}_{Na}$ could be reduced when the activation and deactivation kinetics of the Na$^+$ channel model[3] were altered (by varying the temperature coefficients Q_{10} between 0.6 to 15). The activation time constants (τ_{Na}; single-exponential fit) covered a large range from 5 – 65 µs (voltage protocol indicated below). (**b**) Examples of AIS (solid lines) and somatic APs (dashed lines) with rapid kinetics and low densities of Na$^+$ channels (5 µs and 1,400 pS µm^{-2}), intermediate kinetics and intermediate densities (21 µs and 7,000 pS µm^{-2}), and slow kinetics and high densities (65 µs and 35,000 pS µm^{-2}). While the AP time course in the soma was unaffected by these modifications in axonal Na$^+$ channel kinetics, the AIS spike was strongly affected. (**c**) Impact of Na$^+$ channel kinetics on four different target variables; AP amplitude, AP threshold, dV/dt and the axo-somatic delay. The insets show the area of the target ranges (values from previous study[6]). The overlap of the four different target ranges is shown in black (Merge). In particular the axonal AP amplitude dramatically decreased as the speed of Na$^+$ channel activation was increased in models with a low $\overline{g}_{Na}$. While these simulations show that the fast rate-of-rise of AIS APs may be reproduced in models with fast Na$^+$ channel activation but low $\overline{g}_{Na}$, high $\overline{g}_{Na}$ values $\geq$ 3,000 pS µm^{-2} are required to generate AIS peak amplitudes larger than 80 mV. The estimated $\overline{g}_{Na}$ of 7,000 pS µm^{-2} in the AIS corresponds to about 410 Na$^+$ channels per µm^2 (assuming a 17 pS single-channel conductance[7]). This is well within the range of measured densities at a hippocampal NoR obtained with a highly sensitive quantitative immunolocalization technique using electron microscopic freeze fracturing (346 ± 83 Na$^+$ channels per µm^2)[8]. Furthermore, these Na$^+$ densities are well below the upper limit of ion channel expression as observed for example in the electric organ of the *Torpedo* ray (~20,000 nicotinic acetylcholine receptor channels per µm^{-2}, based on 7 nm average nearest distance[9]).
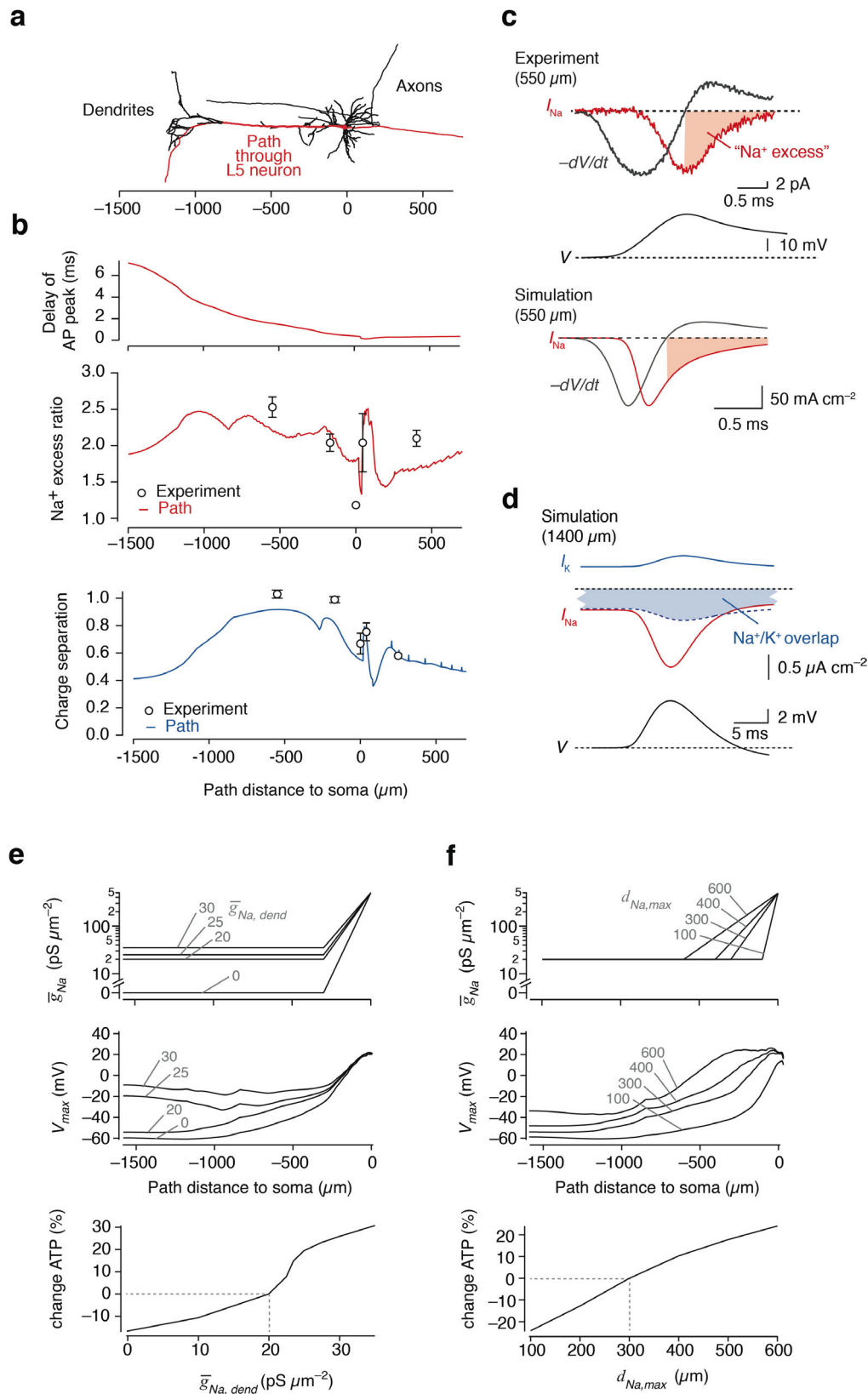
Supplementary Figure 5. Role and dependence of ATP cost to the bAP properties

(**a**) Projection of the 3D morphology of the *in vitro* biocytin-labeled thick-tufted L5 pyramidal NEURON model

with the path for the below shown analysis indicated in red. Negative values correspond to the dendritic and

positive to the axonal path. (**b**) *Bottom*, Delay of the peak of the AP along the above-illustrated path relative to the time of initiation in the AIS. *Middle*, Na$^+$ excess along the path. Note, that the abrupt changes in Na$^+$ excess ratio are not caused by erroneously determined AP peak times but reflect variations in delay of the Na$^+$ influx along the path. The experimentally determined Na$^+$ excess ratios at distal and proximal dendrites, the soma, the AIS, and the distal axon are superimposed as open circles with standard deviation (s.d.) at the corresponding positions (–550, –170, 0, 45, 400 μm, respectively). *Bottom*, charge separation values per segment in the model along the same neuronal path (blue). The experimentally determined charge separation values are superimposed as open circles with s.d. at the corresponding positions (–550, –170, 0, 45, 400 μm, respectively). Note the decreased efficiency in the tuft branches, which is related to the relatively small AP current in face of the persistent currents (see panel d). (**c**) *Top*, experimentally recorded dendritic Na$^+$ excess compared to the time of the peak of a 550 μm dendritic waveform. *Bottom*, Na$^+$ influx overlaid with the dV/dt at 550 μm in the model neuron. (**d**) Na$^+$ and K$^+$ flux in a dendritic tuft section 1400 μm from the soma. Note the presence of persistent Na$^+$ and K$^+$ current flow due to the much more depolarized resting membrane potential in these regions (+13 mV compared to the somatic resting membrane potential). While these persistent currents are very small (note scale), they lead to a significant increase in charge overlap in the tuft regions. (**e**) *Top*, implementation of $\overline{g}_{Na}$ in the apical dendrites. Somatic-to-apical dendritic Na$^+$ channel density decreased linear, reaching the $\overline{g}_{Na,dend}$ value at a distance of 300 μm from the soma ($d_{Na,\max}$). *Middle*, impact of different $\overline{g}_{Na,dend}$ values (0 – 35 pS μm^{-2}) on the dendritic bAP amplitudes. Note the non-linear increase between 20 and 25 pS μm^{-2} due to successful invasion of the daughter tuft branches with higher densities. *Bottom*, non-linear dependence of the global ATP cost in the model neuron on the different $\overline{g}_{Na,dend}$ values. (**f**) *Top*, corresponding implementation of $\overline{g}_{Na}$ in the apical dendrites with different $d_{Na,\max}$ values (between 100 – 600 μm from the soma, $\overline{g}_{Na,dend}$ = 20 pS μm^{-2}). *Middle*, impact of different $d_{Na,\max}$ values on the dendritic bAP amplitudes. *Bottom*, dependence of the global ATP cost in the model neuron on different $d_{Na,\max}$ values. These simulations indicate that within the range of experimentally determined bAP peak amplitudes[10] the global ATP/AP cost varies ± 10%. Furthermore, changing the axonal conduction velocity between 0.28 and 0.53 m s^{-1} (by changing the axonal Na$^+$ channel density between 200 and 1,000 pS μm^{-2}, respectively) resulted in ± 10% of the global ATP/AP (data not shown).

		n^1	n^2	n^4	n^5	n^6	$n^{6.53}$	n^7	n^8	n^{16}	n^{32}	n^{64}	n^{128}	ZHA model	
							Hodgkin-Huxley models							**ZHA model**	
conductance	$\bar{g}_{h1}$ (pS)	5.1	4.8	4.7	4.7	4.6	4.6	4.6	4.6	4.6	4.5	4.5	4.5	4.4	
	$\bar{g}_{h2}$ (pS)	13.5	12.9	12.7	12.6	12.6	12.6	12.6	12.6	12.6	12.6	12.6	12.7	12.4	
activation														α_0 (s⁻¹)	4613
														z_α	0.0
	$A_{\alpha,n}$ (s⁻¹ mV⁻¹)	15.0	25.2	35.9	35.9	35.9	35.9	35.9	48.0	62.1	78.2	93.1	102.7	β_0 (s⁻¹)	19.7
	$A_{\beta,n}$ (s⁻¹)	55.5	62.7	56.1	56.1	56.1	56.1	56.1	42.7	28.4	16.4	8.8	4.6	z_β	1.7
	$B_{\alpha,n}$ (mV)	48.6	53.9	57.8	57.8	57.8	57.8	57.8	58.4	52.9	38.2	23.0	14.3	γ_0 (s⁻¹)	3340
	$C_{\alpha,n}$ (mV)	9.4	10.9	11.8	11.8	11.8	11.8	11.8	13.4	17.5	23.6	28.1	30.3	z_γ	0.7
	$C_{\beta,n}$ (mV)	28.3	36.1	43.5	43.5	43.5	43.5	43.5	49.4	52.0	51.5	51.2	51.4	δ_0 (s⁻¹)	124
														z_δ	0.5
														θ	1.4
inactivation	$A_{\alpha,h1}$ (s⁻¹)	0.0012	0.0013	0.0012	0.0012	0.0012	0.0012	0.0012	0.0013	0.0012	0.0014	0.0013	0.0015	0.0013	
	$A_{\beta,h1}$ (s⁻¹)	5.3	5.7	6.1	6.1	6.1	6.1	6.1	6.2	6.6	6.8	7.0	7.1	6.2	
	$B_{\beta,h1}$ (mV)	66.1	66.2	66.0	66.0	66.0	66.0	66.0	66.1	66.1	66.3	66.3	66.4	66.1	
	$C_{\alpha,h1}$ (mV)	8.7	8.7	8.6	8.6	8.6	8.6	8.6	8.6	8.5	8.6	8.5	8.6	8.6	
	$C_{\beta,h1}$ (mV)	8.0	8.0	8.0	8.0	8.0	8.0	8.0	7.9	7.9	7.9	7.9	7.9	7.9	
	f_{h2}	18.0	19.2	18.9	18.9	18.9	18.9	18.9	18.4	18.2	17.9	17.8	17.7	18.4	
χ^2	χ^2_{act}	1.732	0.686	0.222	0.156	0.122	0.113	0.107	0.100	0.127	0.165	0.186	0.198	0.11	
	χ^2_{SSact}	0.067	0.098	0.146	0.162	0.176	0.183	0.188	0.198	0.258	0.318	0.359	0.381	0.19	
	χ^2_{deact}	0.074	0.086	0.110	0.117	0.123	0.126	0.128	0.132	0.147	0.152	0.153	0.151	0.16	
	χ^2_{inact}	0.443	0.428	0.419	0.417	0.416	0.415	0.414	0.413	0.409	0.408	0.410	0.411	0.41	
	$\chi^2_{SSinact}$	0.140	0.138	0.137	0.138	0.137	0.137	0.138	0.138	0.138	0.139	0.139	0.139	0.14	
	χ^2_{rec}	0.085	0.086	0.086	0.086	0.086	0.086	0.086	0.086	0.086	0.086	0.086	0.086	0.09	
	$\Sigma \chi^2$	2.540	1.521	1.120	1.076	1.061	1.059	1.060	1.067	1.165	1.269	1.332	1.366	1.09	

Supplementary Table 1. Best-fit parameters of HH and ZHA K⁺-models

Parameters of activation and inactivation for the different models (see Online Methods for definitions). Note the steadily changing parameters with increasing number of activation gates, indicating that the global χ^2–minimum during the optimization of the free parameter was reached. The resulting χ^2–values are shown in the lowest row for the 6 analyzed sets of data: activation (*act*, **Fig. 4a**), steady-state activation (*SSact,* **Fig. 3d**), deactivation (*deact,* **Supplementary Fig. 3a**), inactivation (*inact,* **Supplementary Fig. 3b**), steady-state inactivation (*SSinact,* **Fig. 3d**), recovery from inactivation (*rec,* ref. [6]). See also **Supplementary Fig. 3c-f**. The model $n^{6.53}$ is based on a simulation in which the number of activation gates was used as an additional 14th free parameter, yielding 6.53 as best-fit value.

Supplementary References

1. Engel, D. & Jonas, P. Presynaptic action potential amplification by voltage-gated Na$^+$ channels in hippocampal mossy fiber boutons. *Neuron* **45**, 405-417 (2005).

2. Kole, M.H.P.*, et al.* Action potential generation requires a high sodium channel density in the axon initial segment. *Nat. Neurosci.* **11**, 178-186 (2008).

3. Schmidt-Hieber, C. & Bischofberger, J. Fast sodium channel gating supports localized and efficient axonal action potential initiation. *J. Neurosci.* **30**, 10233-10242 (2010).

4. Zagotta, W.N., Hoshi, T. & Aldrich, R.W. Shaker potassium channel gating. III: Evaluation of kinetic models for activation. *J. Gen. Physiol.* **103**, 321-362 (1994).

5. Fleidervish, I.A., Lasser-Ross, N., Gutnick, M.J. & Ross, W.N. Na$^+$ imaging reveals little difference in action potential–evoked Na$^+$ influx between axon and soma. *Nat. Neurosci.* **13**, 852-860 (2010).

6. Kole, M.H.P., Letzkus, J. & Stuart, G. Axon initial segment Kv1 channels control axonal action potential waveform and synaptic efficacy. *Neuron* **55**, 633-647 (2007).

7. Hille, B. *Ionic channels of excitable membranes* (Sinauer Associates, Inc, Sunderland, MA, 2001).

8. Lorincz, A. & Nusser, Z. Molecular identity of dendritic voltage-gated sodium channels. *Science* **328**, 906-909 (2010).

9. Unwin, N. The nicotinic acetylcholine receptor of the Torpedo electric ray. *J. Struct. Biol.* **121**, 181-190 (1998).

10. Stuart, G., Schiller, J. & Sakmann, B. Action potential initiation and propagation in rat neocortical pyramidal neurons. *J. Physiol.* **505**, 617-632 (1997).